ELSEVIER

Journal of Power Sources 101 (2001) 149–157

JOURNAL OF POWER SOURCES

www.elsevier.com/locate/jpowsour

A non-isothermal model of a nickel–metal hydride cell

B. Wu[a], M. Mohammed[b], D. Brigham[b], R. Elder[b], R.E. White[a,*]

[a]*Department of Chemical Engineering, University of South Carolina, Columbia, SC 29208, USA*
[b]*Ford Motor Company, Dearborn, MI, USA*

Received 26 September 2000; accepted 26 December 2000

Abstract

A model for a nickel–metal hydride cell was constructed based on the planar electrode approximation. The mass balances of active species, the kinetics of electrochemical reactions, the ohmic effects of internal resistance, and the energy balance of the whole cell were considered in the model. An empirical approach was utilized to account for the hysteresis potential behavior of the nickel electrode. The model predictions showed favorable agreement with the experimental data.

Keywords: Nickel–metal hydride battery; Battery modeling; Nickel electrode; Hysteresis potential behavior

1. Introduction

The nickel–metal hydride battery is one of the latest battery technologies. The nickel–metal hydride battery has some advantages, e.g. higher energy density and environmental friendliness, over the more commonly used rechargeable batteries (such as the lead-acid battery and the nickel–cadmium battery). However, it also has some disadvantages, e.g. higher cost and higher self-discharge.

A nickel–metal hydride cell module (Fig. 1) consists of three major components: the positive nickel electrode, the nylon separator, and the negative metal hydride electrode. Generally, both the nickel electrode and the metal hydride electrode are thin porous electrodes. In a nickel–metal hydride cell, the nickel electrode determines the cell capacity and the metal hydride electrode determines the cell cycle life.

Normally, the metal hydride electrode is pre-charged (i.e. has residue charge when the cell is fully discharged) to avoid oxygen gas generation during over discharge and has extra capacity to avoid hydrogen gas generation during overcharge. Since the metal hydride material gradually loses capacity through usage due to the corrosion by the KOH electrolyte, the extra capacity in the metal hydride electrode also reduces the rate at which the capacity is lost in the cell.

The electrolyte in a nickel–metal hydride cell is concentrated KOH solution, which has good electric conductivity for a wide range of temperatures. Some LiOH is usually added to the electrolyte to improve the performance of the electrodes.

In the normal operation of a nickel–metal hydride cell, there are four major reactions, as listed below.

Positive nickel electrode:

$$\mathrm{NiOOH} + \mathrm{H_2O} + \mathrm{e^-} \underset{\text{charge}}{\overset{\text{discharge}}{\rightleftarrows}} \mathrm{Ni(OH)_2} + \mathrm{OH^-} \tag{1}$$

$$2\mathrm{OH^-} \rightarrow \tfrac{1}{2}\mathrm{O_2} + \mathrm{H_2O} + 2\mathrm{e^-} \tag{2}$$

Negative metal hydride electrode:

$$\mathrm{MH} + \mathrm{OH^-} \underset{\text{charge}}{\overset{\text{discharge}}{\rightleftarrows}} \mathrm{H_2O} + \mathrm{M} + \mathrm{e^-} \tag{3}$$

$$\tfrac{1}{2}\mathrm{O_2} + \mathrm{H_2O} + 2\mathrm{e^-} \rightarrow 2\mathrm{OH^-} \tag{4}$$

There is a main and a side reaction at each of the electrodes. The main reaction at the positive electrode is the redox reaction of the nickel active material and at the negative electrode the redox reaction of the metal hydride material. The side reaction at the positive electrode is oxygen evolution and at the negative electrode oxygen reduction. The two side reactions are coupled together by the oxygen transport from the positive electrode to the negative electrode.

With the rapid development of computer technology, modeling and simulation has become an indispensable approach in the design and optimization of many engineering systems. For batteries, the modeling and simulation can be used to: (i) analyze the influence of some physical parameters (e.g. electrode thickness and particle size) on battery behavior for design optimizations and scale-up investigations; (ii) predict battery behavior under different

* Corresponding author. Tel.: +1-803-777-3270; fax: +1-803-777-8265.
E-mail address: white@engr.sc.edu (R.E. White).

0378-7753/01/$ – see front matter
PII: S0378-7753(01)00788-1

Nomenclature

a_{neg}	specific surface area of the negative electrode (cm^2/cm^3)
a_{pos}	specific surface area of the positive electrode (cm^2/cm^3)
A_{cell}	total surface area of the cell (cm^2)
A_{neg}	total geometry area of the negative electrode (cm^2)
A_{pos}	total geometry area of the positive electrode (cm^2)
c_e	concentration of KOH electrolyte (mol/cm^3)
$c_{e,ref}$	reference concentration of KOH electrolyte (mol/cm^3)
c_{H^+}	concentration of nickel hydroxide in nickel active material (mol/cm^3)
$c_{H^+,max}$	maximum concentration of nickel hydroxide in nickel active material (mol/cm^3)
$c_{H^+,ref}$	reference concentration of nickel hydroxide in nickel active material (mol/cm^3)
c_{MH}	concentration of hydrogen in metal hydride material (mol/cm^3)
$c_{MH,max}$	maximum concentration of hydrogen in metal hydride material (mol/cm^3)
$c_{MH,ref}$	reference concentration of hydrogen in metal hydride material (mol/cm^3)
c_p	heat capacity of the cell (J/g/K)
$E_{a,k}$	activation energy of reaction k (J)
f	function of reactant concentrations
F	Faraday's constant (96,487 C/eq)
h	heat transfer coefficient between the cell and the environment ($W/cm^2/K$)
i_{cell}	current of the nickel–metal hydride cell (A)
$i_{o,k}$	exchange current density of reaction k (A/cm^2)
$i_{o,k,ref}$	exchange current density of reaction k at reference reactant concentrations (A/cm^2)
$i_{k,ref}$	limiting-current density of reaction k at reference reactant concentrations (A/cm^2)
j_k	current density of reaction k (A/cm^2)
k_c	parameter in the empirical hysteresis equation for the charge process
k_d	parameter in the empirical hysteresis equation for the discharge process
k_o	parameter in the empirical hysteresis equation for the open-circuit process
l_{neg}	thickness of the negative electrode (cm)
l_{pos}	thickness of the positive electrode (cm)
$l_{y,neg}$	effective thickness of the layer of metal hydride material (cm)
$l_{y,pos}$	effective thickness of the layer of nickel active material (cm)
L_{MH}	loading of metal hydride material (g/cm^2)
$L_{Ni(OH)_2}$	loading of nickel active material (g/cm^2)
m_{cell}	mass of the cell (g)
p_{O_2}	oxygen pressure in a nickel–metal hydride cell (atm)
$p_{O_2,ref}$	reference oxygen pressure in a nickel–metal hydride cell (atm)
R	universal gas constant (8.3143 J/mol/K or 82.0562 atm cm^3/mol/K)
R_{int}	internal ohmic resistance of the nickel–metal hydride cell (Ω)
SOC	state of charge
t	time (s)
T	temperature (K)
T_0	room temperature (298.15 K)
U_k	equilibrium potential of reaction k at standard conditions (V)
$U_{1,c}$	apparent open-circuit potential of the redox reaction of nickel active material at standard conditions during the whole range charge process (V)
$U_{1,d}$	apparent open-circuit potential of the redox reaction of nickel active material at standard conditions during the whole range discharge process (V)
v_{cell}	potential of a nickel–metal hydride cell (V)
V_{gas}	gas volume in a nickel–metal hydride cell (cm^3)

Greeks letters

$\Delta\phi_{neg}$	potential difference at the solid–liquid interface on the negative electrode (V)
$\Delta\phi_{pos}$	potential difference at the solid–liquid interface on the positive electrode (V)
ϕ^o_{eq}	apparent open-circuit potential at the starting point of a process (V)
$\phi_{eq,k}$	equilibrium potential of reaction k (V)
$\phi_{eq,1,c}$	apparent open-circuit potential of the redox reaction of nickel active material during the whole range charge process (V)
$\phi_{eq,1,d}$	apparent open-circuit potential of the redox reaction of nickel active material during the whole range discharge process (V)
$\phi_{h,c}$	transient hysteresis potential of the redox reaction of nickel active material during the charge process (V)
$\phi_{h,d}$	transient hysteresis potential of the redox reaction of nickel active material during the discharge process (V)
$\phi_{h,o}$	transient hysteresis potential of the redox reaction of nickel active material during the open-circuit process (V)
$\phi_{neg,l}$	potential in the liquid electrolyte on the negative electrode (V)
$\phi_{neg,s}$	potential in the solid metal hydride material on the negative electrode (V)
$\phi_{pos,l}$	potential in the liquid electrolyte on the positive electrode (V)
$\phi_{pos,s}$	potential in the solid nickel active material on the positive electrode (V)
$\rho_{Ni(OH)_2}$	density of nickel active material (g/cm^3)
ρ_{MH}	density of metal hydride material (g/cm^3)

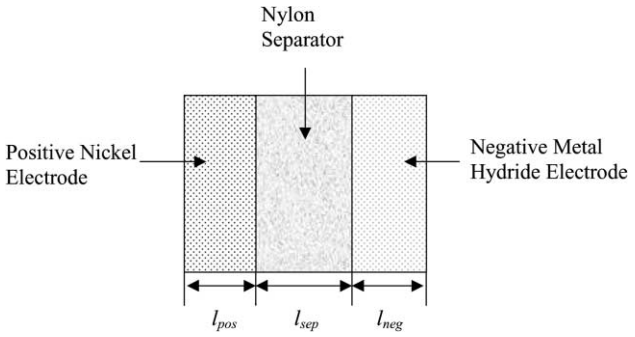

Fig. 1. Schematic diagram of a NiMH cell module.

operating conditions (e.g. charge/discharge rate and cut-off voltage) for operation optimizations; and (iii) investigate unclear physical/chemical mechanisms by comparing the model predictions with extensive experimental data.

The nickel electrode has been used and researched for a long time [1–6]. However, well-established theories for some characteristics of the nickel electrode (e.g. second discharge plateau [7] and hysteresis potential behavior [8]) are still not currently available. A significant amount of modeling work has been done over the years on the nickel electrode either alone or in a battery [9–14]. The most comprehensive model for the nickel electrode is a pseudo-2D model with considerations of both the processes across the macroscopic electrode dimension and the processes inside the microscopic nickel active material layer.

Some modeling efforts on the metal hydride electrode have been conducted in recent years [15–18]. A pseudo-2D model of the metal hydride electrode similar to that of the nickel electrode was also utilized.

However, very limited modeling work is reported in the literature for the complete nickel–metal hydride cell. Paxton and Newman [19] developed a discharge model of a nickel–metal hydride cell. They found that the proton diffusion in the nickel active material could be neglected at normal charge/discharge rates. Based on their model, some optimizations of cell design with respect to the electrode thickness and porosity were conducted. Later, Gu et al. [20] constructed a more comprehensive model for a nickel–metal hydride cell. The oxygen reactions on both the positive and negative electrodes were included in their model. Using their model, the effects of the oxygen evolution rate and the charge/discharge rate on the cell behavior were investigated.

The model developed by Paxton and Newman [19] and the one by Gu et al. [20] are both isothermal ones. However, in reality, significant heat effects are involved in the operation of a battery, and many processes in a battery are very sensitive to temperature changes. Thus, it is highly desirable to include the thermal effects in a nickel–metal hydride cell model.

Furthermore, these two models used a reversible electrochemical reaction to describe the behavior of the nickel active material. However, the potential behavior of the nickel active material shows significant hysteresis features that cannot be described by a reversible electrochemical reaction. Thus, for some operating conditions, there may be significant prediction errors with these two models.

In general, the number of details to be considered in a nickel–metal hydride cell will determine the complexity of the model to be constructed. The more details considered in the model, the more parameters and equations will appear, and the more complex and computational intensive the model program will become. For the nickel–metal hydride battery, the following hierarchy of models could be constructed:

1. Empirical model: fitted equations from experimental data.
2. Lumped model (with the planar electrode approximation): equations of mass balance, charge balance, electrochemical kinetics, and energy balance, etc.
3. Distributed model (with 1D or pseudo-2D porous electrode models): equations in (2) plus equations of distributed processes.
4. Coupled electrochemical/thermal model: equations in (1), (2), and (3) plus the heat transfer equations in multiple dimensions.

The primary objective of this work is to provide a model of a nickel–metal hydride cell for power system simulations. Since, many models of different devices need to be solved together in a system simulation, the battery model must be simple enough to make the whole system simulation computationally feasible. As a result, the lumped modeling approach was used in this work. The advantages of this approach are (i) the model is based on first-principle mechanisms; (ii) model equations are simple to solve; and (iii) the model can be easily incorporated into a system model or a thermal model. The disadvantages of this approach are (i) model assumptions may not be valid under some situations; and (ii) effects of many cell parameters cannot be evaluated.

2. Governing equations of the model

The model presented here uses the planar electrode approximation, i.e. each electrode is treated as a huge planar electrode with a surface area equal to the total internal surface area of the porous electrode. Since, battery electrodes are normally made very thin to minimize ohmic effects, a planar electrode model usually gives insignificant errors and costs much less computation compared to a rigorous porous electrode model.

The kinetics of reactions (Eqs. (1)–(3)) are described with the Butler–Volmer equation.

$$j_1 = i_{o,1}\left[\exp\left(\frac{0.5F}{RT}(\Delta\phi_{pos} - \phi_{eq,1})\right) - \exp\left(-\frac{0.5F}{RT}(\Delta\phi_{pos} - \phi_{eq,1})\right)\right] \quad (5)$$

$$j_2 = i_{o,2}\left[\exp\left(\frac{F}{RT}(\Delta\phi_{pos} - \phi_{eq,2})\right) - \exp\left(-\frac{F}{RT}(\Delta\phi_{pos} - \phi_{eq,2})\right)\right] \quad (6)$$

$$j_3 = i_{o,3}\left[\exp\left(\frac{0.5F}{RT}(\Delta\phi_{neg} - \phi_{eq,3})\right) - \exp\left(-\frac{0.5F}{RT}(\Delta\phi_{neg} - \phi_{eq,3})\right)\right] \quad (7)$$

The potential differences at the solid–liquid interface on the electrodes are given by

$$\Delta\phi_{pos} = \phi_{pos,s} - \phi_{pos,l} \quad (8)$$

$$\Delta\phi_{neg} = \phi_{neg,s} - \phi_{neg,l} \quad (9)$$

The exchange current densities in Eqs. (5)–(7) can be calculated from the reference states

$$i_{o,1} = i_{o,1,ref}\left(\frac{c_{H^+}}{c_{H^+,ref}}\right)^{0.5}\left(\frac{c_e}{c_{e,ref}}\right)^{0.5}\left(\frac{c_{H^+,max} - c_{H^+}}{c_{H^+,max} - c_{H^+,ref}}\right)^{0.5} \exp\left(\frac{E_{a,1}}{R}\left(\frac{1}{T} - \frac{1}{T_0}\right)\right) \quad (10)$$

$$i_{o,2} = i_{o,2,ref}\left(\frac{c_e}{c_{e,ref}}\right)^{2}\left(\frac{p_{O_2}}{p_{O_2,ref}}\right)^{0.5} \exp\left(\frac{E_{a,2}}{R}\left(\frac{1}{T} - \frac{1}{T_0}\right)\right) \quad (11)$$

$$i_{o,3} = i_{o,3,ref}\left(\frac{c_{MH}}{c_{MH,ref}}\right)^{0.5}\left(\frac{c_e}{c_{e,ref}}\right)^{0.5}\left(\frac{c_{MH,max} - c_{MH}}{c_{MH,max} - c_{MH,ref}}\right)^{0.5} \exp\left(\frac{E_{a,3}}{R}\left(\frac{1}{T} - \frac{1}{T_0}\right)\right) \quad (12)$$

For the nickel active material, the hysteresis potential behavior exists, i.e. the charge and discharge potential curves form hysteresis loops. In this work, an empirical approach has been used to characterize the hysteresis potential. For the whole range of charge and discharge processes, two apparent open-circuit potential curves based on the Nernst equation are utilized.

$$\phi_{eq,1,c} = U_{1,c} + (T - T_0)\frac{dU_{1,c}}{dT} + \frac{RT}{F}\ln\left(\frac{c_{H^+,max} - c_{H^+}}{c_e c_{H^+}}\right) \quad (13)$$

$$\phi_{eq,1,d} = U_{1,d} + (T - T_0)\frac{dU_{1,d}}{dT} + \frac{RT}{F}\ln\left(\frac{c_{H^+,max} - c_{H^+}}{c_e c_{H^+}}\right) \quad (14)$$

However, when switching between different processes, there is a relaxation process before the ideal charge/discharge potential curves are reached, as shown in Figs. 2 and 3. Three empirical equations are used in this work to represent this relaxation process.

$$\phi_{h,c} = \phi^o_{eq} + (\phi_{eq,1,c} - \phi^o_{eq})(1 - e^{-k_c|i_{cell}|(t-t^0)}) \quad (15)$$

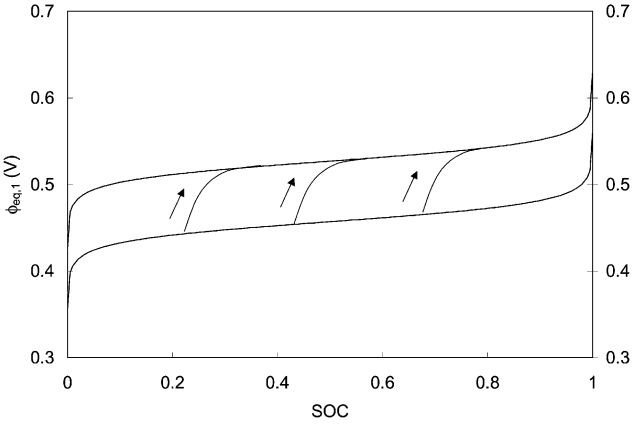

Fig. 2. Qualitative diagram of hysteresis potential behavior for the charge process.

$$\phi_{h,d} = \phi^o_{eq} + (\phi_{eq,1,d} - \phi^o_{eq})(1 - e^{-k_d|i_{cell}|(t-t^0)}) \quad (16)$$

$$\phi_{h,o} = \phi^o_{eq} + (\phi_{eq,1,d} - \phi^o_{eq})(1 - e^{-k_o(t-t^0)}) \quad (17)$$

In the above equations ϕ^o_{eq} is the value at the starting time. The values for parameters k_c, k_d, and k_o can be determined from the experimental data.

The equilibrium potential for the oxygen reactions is given by

$$\phi_{eq,2} = U_2 + (T - T_0)\frac{dU_2}{dT} + \frac{RT}{2F}\ln\left(\frac{p^{1/2}_{O_2}}{c^2_e}\right) \quad (18)$$

while the equilibrium potential for the metal hydride reaction is expressed by Paxton and Newman [19]

$$\phi_{eq,3} = U_3 + (T - T_0)\frac{dU_3}{dT} - \frac{RT}{F}\ln c_e + 9.712 \times 10^{-4} + 0.23724\exp\left(-\frac{28.057 c_{MH}}{c_{MH,max}}\right) - \frac{2.7302 \times 10^{-4}}{[(c_{MH}/c_{MH,max})^2 + 0.010768]} \quad (19)$$

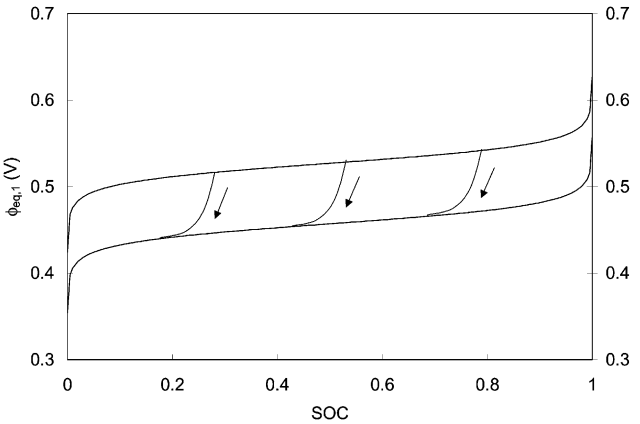

Fig. 3. Qualitative diagram of hysteresis potential behavior for the discharge process.

Due to the huge electrochemical driving force for oxygen reduction on the negative electrode, a limiting-current equation is used for the rate of reaction Eq. (4).

$$j_4 = -\frac{p_{O_2}}{p_{O_2,ref}} i_{4,ref} \exp\left(\frac{E_{a,4}}{R}\left(\frac{1}{T}-\frac{1}{T_0}\right)\right) \quad (20)$$

The charge balances on the electrodes are described by

$$i_{cell} = A_{pos} a_{pos} l_{pos} (j_1 + j_2) \quad (21)$$

$$-i_{cell} = A_{neg} a_{neg} l_{neg} (j_3 + j_4) \quad (22)$$

The mass balance of the nickel active material is given by

$$l_{y,pos} \frac{dc_{H^+}}{dt} = -\frac{j_1}{F} \quad (23)$$

where the effective thickness of the nickel active material is

$$l_{y,pos} = \frac{L_{Ni(OH)_2}}{\rho_{Ni(OH)_2} l_{pos} a_{pos}} \quad (24)$$

The mass balance of metal hydride material is given by

$$l_{y,neg} \frac{dc_{MH}}{dt} = -\frac{j_4}{F} \quad (25)$$

where the effective thickness of metal hydride active material is

$$l_{y,neg} = \frac{L_{MH}}{\rho_{MH} l_{neg} a_{neg}} \quad (26)$$

The mass balance of oxygen is described by

$$\frac{V_{gas}}{RT}\frac{dp_{O_2}}{dt} = \frac{(A_{pos} a_{pos} l_{pos} j_2 + A_{neg} a_{neg} l_{neg} j_4)}{F} \quad (27)$$

The separator is treated as an ohmic resistance, which gives

$$i_{cell} R_{int} = \phi_{pos,l} - \phi_{neg,l} \quad (28)$$

The cell potential is calculated by

$$v_{cell} = \phi_{pos,s} - \phi_{neg,s} = \Delta\phi_{pos} - \Delta\phi_{neg} + i_{cell} R_{int} \quad (29)$$

The energy balance of the whole cell is described by

$$c_p m_{cell} \frac{dT}{dt} = -hA_{cell}(T - T_a) + i_{cell} v_{cell} - \sum_{k=1,4} j_k \left(\phi_{eq,k} - T\frac{d\phi_{eq,k}}{dT}\right) \quad (30)$$

Since, the following equations hold

$$\phi_{eq,k} = U_k + (T - T_0)\frac{dU_k}{dT} + Tf(c) \quad (31)$$

$$\frac{d\phi_{eq,k}}{dT} = \frac{dU_k}{dT} + f(c) \quad (32)$$

we have

$$\phi_{eq,k} - T\frac{d\phi_{eq,k}}{dT} = U_k - T_0\frac{dU_k}{dT} \quad (33)$$

Substitution of Eq. (33) into Eq. (30) yields

$$c_p m_{cell} \frac{dT}{dt} = -hA_{cell}(T - T_a) + i_{cell} v_{cell} - \sum_{k=1,4} j_k \left(U_k - T_0\frac{dU_k}{dT}\right) \quad (34)$$

The SOC of the cell is given by the charged state of the nickel active material

$$SOC = 1 - \frac{c_{H^+}}{c_{H^+,max}} \quad (35)$$

Given the applied current on the cell i_{cell}, there are seven dependent variables (v_{cell}, c_{H^+}, c_{MH}, p_{O_2}, $\Delta\phi_{pos}$, $\Delta\phi_{neg}$, and T) that need to be solved with the model. The procedure used for serial simulation of electrochemical systems, based on two FORTRAN solvers DAEIS and DASRT, has been used to simulate the nickel–metal hydride cell undergoing many processes [21].

3. Results and discussion

The parameter values used in the model are those of a 4.5 Ah (rated capacity) nickel–metal hydride cell produced by VARTA Battery AG (www.varta.com). These values are listed in Table 1. The actual cell capacity after some cycling is close to 5.3 Ah. The experimental data was generated during testing at the Ford Motor Company Scientific Research Laboratory, in Dearborn, Michigan, USA, using a BTS-600 Firing Circuits battery tester and software. Where possible, the model predicted values and the actual test values are overlain in the figures presented.

The cell potential with respect to time for three processes is shown in Fig. 4. The high potential plateau at the end of the charge process corresponds to the overcharge period when the oxygen evolution and reduction reactions dominate. Since, the rate of oxygen evolution is much slower

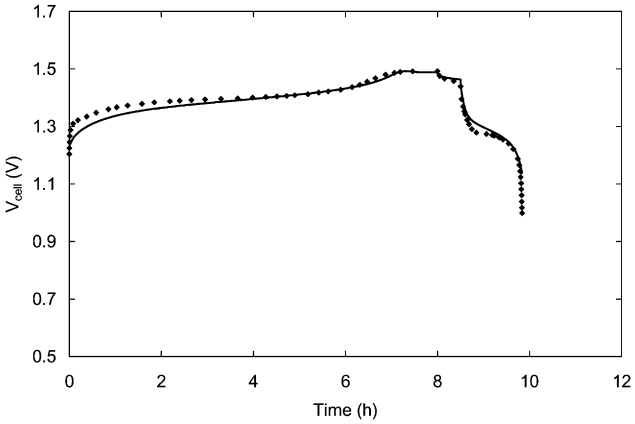

Fig. 4. Cell potential for the following processes (model predictions in line): 0.8 A charge for 8 h, open-circuit for 0.5 h, and 4.0 A discharge to 1.0 V.

Table 1
Parameters used for the model of a nickel–metal hydride cell

Parameter	Value
a_{pos} (cm^2/cm^3)	4000.0
a_{neg} (cm^2/cm^3)	3000.0
A_{pos} (cm^2)	325.0
A_{neg} (cm^2)	360.0
A_{cell} (cm^2)	77.0
c_e (mol/cm^3)	7.0×10^{-3}
$c_{e,ref}$ (mol/cm^3)	1.0×10^{-3}
$c_{MH,max}$ (mol/cm^3)	1.0×10^{-1}
$c_{MH,ref}$ (mol/cm^3)	0.5 ($c_{MH,max}$)
$c_{H^+,max}$ (mol/cm^3)	3.7×10^{-2}
$c_{H^+,ref}$	0.5 ($c_{Ni(OH)_2,max}$)
$i_{0,1,ref}$ (A/cm^2)	1.0×10^{-4}
$i_{0,2,ref}$ (A/cm^2)	2.0×10^{-11}
$i_{0,3,ref}$ (A/cm^2)	1.0×10^{-4}
$i_{4,ref}$ (A/cm^2)	1.0×10^{-4}
k_c	1.0×10^{-3}
k_d	1.0×10^{-3}
k_o	1.0×10^{-2}
$E_{a,1}$ (kJ/mol)	10
$E_{a,2}$ (kJ/mol)	120
$E_{a,3}$ (kJ/mol)	10
$E_{a,4}$ (kJ/mol)	10
l_{pos} (cm)	3.3×10^{-2}
l_{neg} (cm)	2.8×10^{-2}
$L_{Ni(OH)_2}$ (g/cm^2)	6.8×10^{-2}
L_{MH} (g/cm^2)	1.13×10^{-1}
$p_{O_2,ref}$ (atm)	1.0
R_{int} (Ω)	5.0×10^{-3}
T_0 (K)	298.15
$U_{1,c}$ (V)	0.527
$U_{1,d}$ (V)	0.427
U_2 (V)	0.4011
U_3 (V)	−0.8279
U_4 (V)	0.4011
dU_1/dT (mV/K)	−1.35
dU_2/dT (mV/K)	−1.68
dU_3/dT (mV/K)	−1.55
dU_4/dT (mV/K)	−1.68
V_{gas} (cm^3)	1.0×10^{-1}
$\rho_{Ni(OH)_2}$ (g/cm^3)	3.4
ρ_{MH} (g/cm^3)	7.49

than that of the nickel reaction, a higher overpotential is needed to maintain the same charge rate. It is observed that the cell was overcharged for more than 2 h. The full capacity of the cell can be easily determined from the discharge process of this operation.

The cell temperature with respect to time is shown in Fig. 5. The heat generation at the early stage of the charge process is insignificant. During the overcharge period, since almost all the input energy is wasted on heat generation, there is a rapid increase in cell temperature. At the end of the discharge process, the depletion of reactants results in high overpotential loss that also causes a cell temperature increase. It is worth mentioning that hydrogen absorption into the metal hydride material is an exothermal process, while hydrogen release from the metal hydride material is an endothermic process. This has significant influence on the thermal behavior of the whole nickel–metal hydride cell and can be observed at low charge/discharge rates.

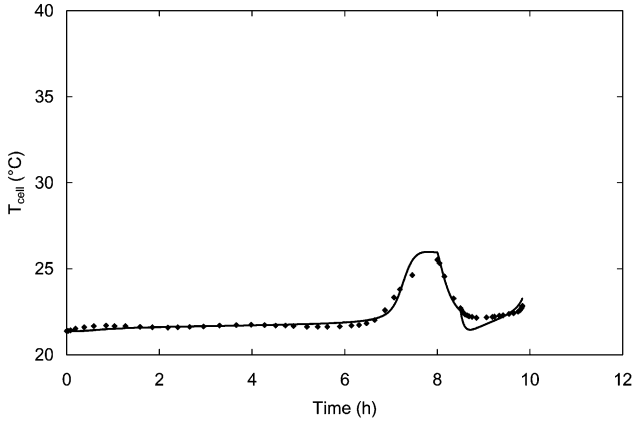

Fig. 5. Cell temperature for the following processes (model predictions in line): 0.8 A charge for 8 h, open-circuit for 0.5 h, and 4.0 A discharge to 1.0 V.

The mole fractions of the charged species on the positive and negative electrodes with respect to time are shown in Fig. 6. During the early period of the charge process and the entire discharge process, nearly constant-slope lines are obtained for these mole fractions. This indicates that side reactions are insignificant during these periods.

A 5% pre-charge on the metal hydride electrode is used in the simulation. It should be noted that less than half of the metal hydride material is utilized. During the overcharge period, there is little if any increase in cell capacity. This is due to the dominance of oxygen side reactions that consume almost all the input current.

The cell potential with respect to time for three different operations is shown in Fig. 7. In these three operations, the open-circuit and discharge processes are the same, but the charge rate is different for all three. While there is good

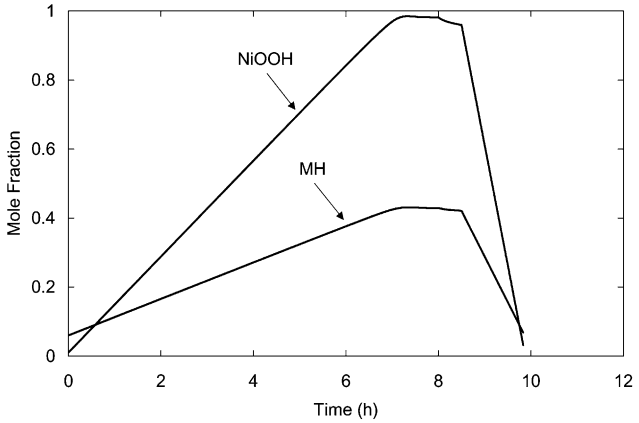

Fig. 6. Model predicted mole fractions of charged active material on the positive and negative electrodes for the following processes: 0.8 A charge for 8 h, open-circuit for 0.5 h, and 4.0 A discharge to 1.0 V.

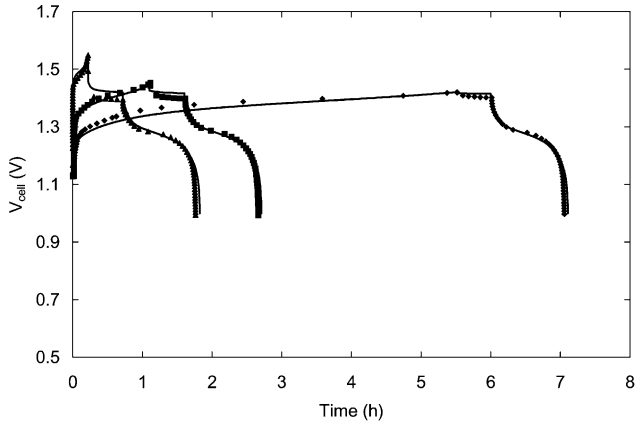

Fig. 7. Cell potential for three operations (model predictions in line): (i) 20.0 A charge for 0.22 h, open-circuit for 0.5 h, and 4.0 A discharge to 1.0 V; (ii) 4.0 A charge for 1.1 h, open-circuit for 0.5 h, and 4.0 A discharge to 1.0 V; and (iii) 0.8 A charge for 5.5 h, open-circuit for 0.5 h, and 4.0 A discharge to 1.0 V.

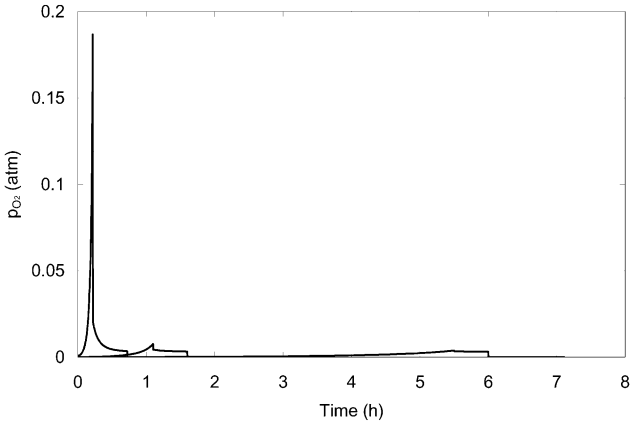

Fig. 9. Model predicted oxygen pressure in the cell for three operations: (i) 20.0 A charge for 0.22 h, open-circuit for 0.5 h, and 4.0 A discharge to 1.0 V; (ii) 4.0 A charge for 1.1 h, open-circuit for 0.5 h, and 4.0 A discharge to 1.0 V; and (iii) 0.8 A charge for 5.5 h, open-circuit for 0.5 h, and 4.0 A discharge to 1.0 V.

correlation between the model predictions and the experimental data for the charge and discharge processes, some errors are noted for the open-circuit process. This indicates that efforts to improve the model should concentrate on providing a better description of the open-circuit process.

At high charge rates, due to the high ohmic and overpotential losses, high charge potential is needed as expected. It is worth mentioning that the Varta nickel–metal hydride cell performs well even at a 30 C charge rate. Thus, the solid phase diffusion limitation is unlikely to be important in the cell at normal charge rates.

The cell temperature with respect to time for the same operations is given in Fig. 8. At high charge rates, the cell heat generation is significant due to high ohmic and overpotential losses, which may cause the cell temperature rise more than 10°C. Since, the cell is not fully charged for the given operations, it can be expected that overcharge will cause a even more significant rise of the cell temperature at high charge rates, which may cause thermal safety problems.

The model predicted oxygen pressure in the cell is given in Fig. 9. It is observed that at high charge rates, the oxygen pressure rise can be significant at the end of the charge process. There is negligible oxygen pressure during the discharge process.

The cell potential with respect to time for three different operations is shown in Fig. 10. In these operations the charge, and open-circuit processes are the same, but the discharge process is different for all three operations. As expected, low discharge potential is resulted at high discharge rates due to the high ohmic and overpotential losses. A S-bend discharge curve is shown at all three discharge rates. Since, the cell is not discharged from the fully charged

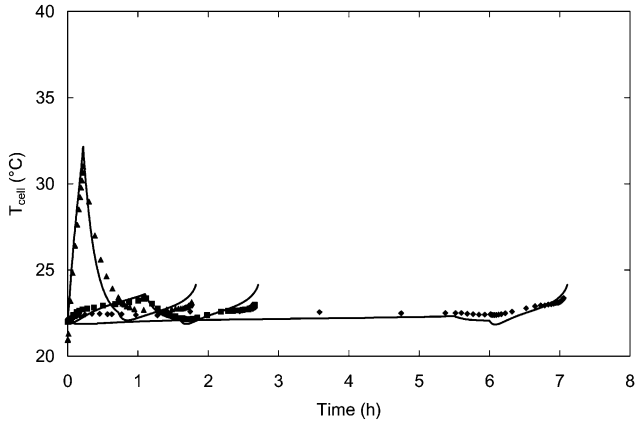

Fig. 8. Cell temperature for three operations (model predictions in line): (i) 20.0 A charge for 0.22 h, open-circuit for 0.5 h, and 4.0 A discharge to 1.0 V; (ii) 4.0 A charge for 1.1 h, open-circuit for 0.5 h, and 4.0 A discharge to 1.0 V; and (iii) 0.8 A charge for 5.5 h, open-circuit for 0.5 h, and 4.0 A discharge to 1.0 V.

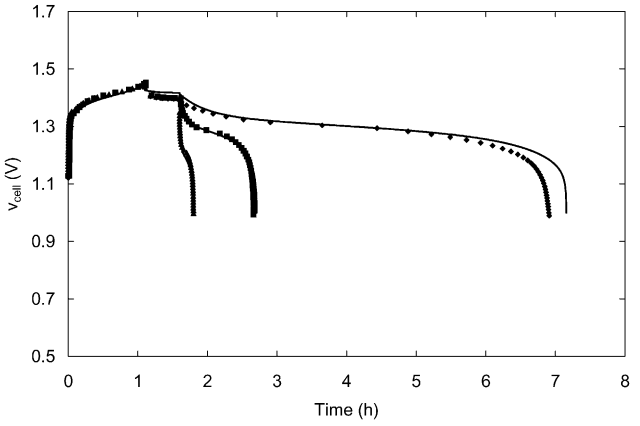

Fig. 10. Cell potential for three operations (model predictions in line): (i) 4.0 A charge for 1.1 h, open-circuit for 0.5 h, and 20.0 A discharge to 1.0 V; (ii) 4.0 A charge for 1.1 h, open-circuit for 0.5 h, and 4.0 A discharge to 1.0 V; and (iii) 4.0 A charge for 1.1 h, open-circuit for 0.5 h, and 0.8 A discharge to 1.0 V.

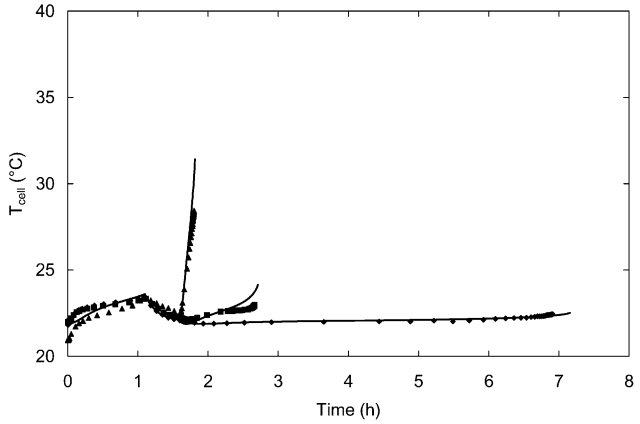

Fig. 11. Cell temperature for three operations (model predictions in line): (i) 4.0 A charge for 1.1 h, open-circuit for 0.5 h, and 20.0 A discharge to 1.0 V; (ii) 4.0 A charge for 1.1 h, open-circuit for 0.5 h, and 4.0 A discharge to 1.0 V; and (iii) 4.0 A charge for 1.1 h, open-circuit for 0.5 h, and 0.8 A discharge to 1.0 V.

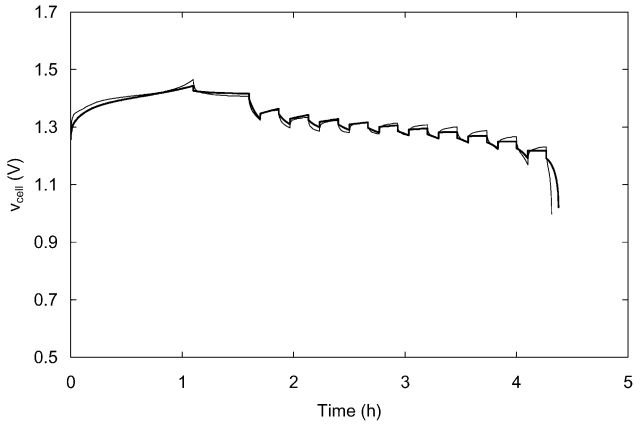

Fig. 13. Cell potential for the following processes (model predictions in thick line): 4.0 A charge for 1.1 h and open-circuit for 0.5 h, and repeat (4.0 A discharge for 0.11 h and open-circuit for 0.167 h) for 10 times, and 4.0 A discharge to 1.0 V.

state, the Nernst equation will predict a lower potential at the early discharge period. The higher potential at the early stage of the discharge process is actually an effect of the hysteresis phenomenon, i.e. potential relaxation when switching processes.

The cell temperature for the same operations is given in Fig. 11. At high discharge rates, the cell heat generation is significant due to high ohmic and overpotential losses, and that causes sharp cell temperature rises. Thus, good thermal management is needed if high discharge rates are used to avoid a thermal run-away situation.

The cell potential with respect to time for a series of pulse charge/open-circuit operations followed by an open-circuit and a discharge process is shown in Fig. 12. The cell potential with respect to time for a charge process followed by an open-circuit, and then a series of pulse discharge/open-circuit operations is shown in Fig. 13. The potential difference between the pulse charge/discharge processes and the following open-circuit processes is mainly the effects of ohmic resistance. However, careful comparison shows that the open-circuit potential is different between pulse charge and pulse discharge operations at corresponding cell SOC. This potential difference gives a clear demonstration of the significance of the hysteresis phenomenon. This behavior has been satisfactorily reflected with the model.

The cell potential with respect to time for five different operations is shown in Fig. 14. In these operations, the cell is charged to different SOC levels (at the same charge rate) and then it is discharged at the same rate after the same open-circuit period. It is observed that the cell discharge potential is higher than that predicted by the Nernst equation, especially when discharging from a lower SOC. This is a typical

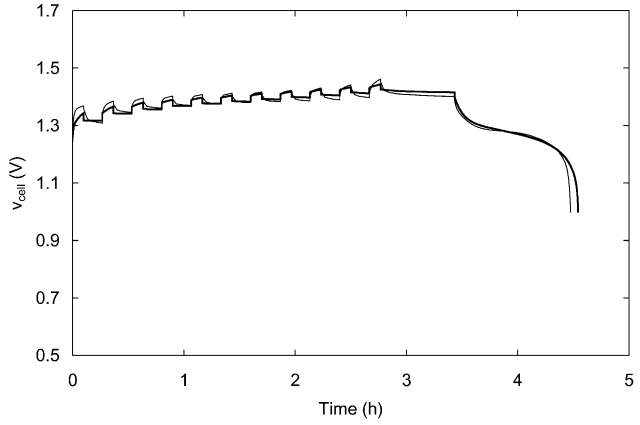

Fig. 12. Cell potential for the following processes (model predictions in thick line): repeat (4.0 A charge for 0.11 h and open-circuit for 0.167 h) for 11 times, open-circuit for 0.5 h, and 4.0 A discharge to 1.0 V.

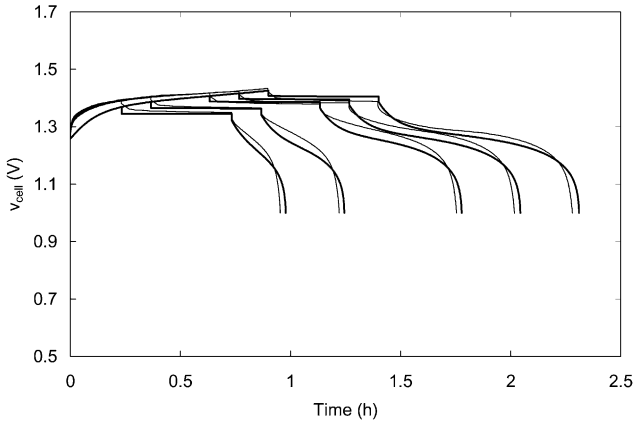

Fig. 14. Cell potential for the following five different operations (model predictions in thick line): (i) 4.0 A charge for 14 min, open-circuit for 30 min, and 4.0 A discharge to 1.0 V; (ii) 4.0 A charge for 22 min, open-circuit for 30 min, and 4.0 A discharge to 1.0 V; (iii) 4.0 A charge for 38 min, open-circuit for 30 min, and 4.0 A discharge to 1.0 V; (iv) 4.0 A charge for 46 min, open-circuit for 30 min, and 4.0 A discharge to 1.0 V; and (v) 4.0 A charge for 54 min, open-circuit for 30 min, and 4.0 A discharge to 1.0 V.

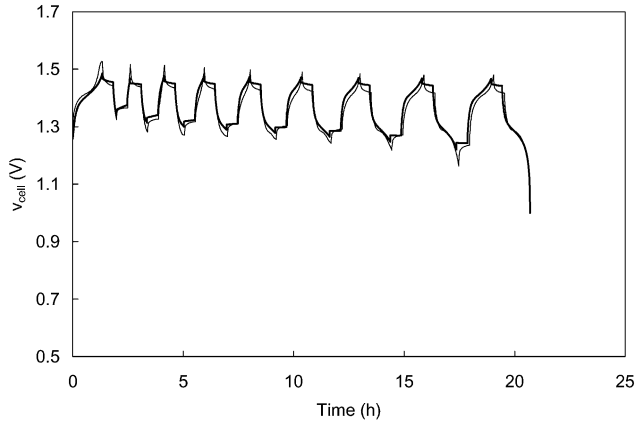

Fig. 15. Cell potential for the following processes (model predictions in thick line): 4.0 A charge for 80 min, open-circuit for 30 min, 4.0 A discharge for 8 min, open-circuit for 30 min, 4.0 A charge for 8 min, open-circuit for 30 min, 4.0 A discharge for 16 min, open-circuit for 30 min, 4.0 A charge for 16 min, open-circuit for 30 min, 4.0 A discharge for 24 min, open-circuit for 30 min, 4.0 A charge for 24 min, open-circuit for 30 min, 4.0 A discharge for 32 min, open-circuit for 30 min, 4.0 A charge for 32 min, open-circuit for 30 min, 4.0 A discharge for 40 min, open-circuit for 30 min, 4.0 A charge for 40 min, open-circuit for 30 min, 4.0 A discharge for 48 min, open-circuit for 30 min, 4.0 A charge for 48 min, open-circuit for 30 min, 4.0 A discharge for 56 min, open-circuit for 30 min, 4.0 A charge for 56 min, open-circuit for 30 min, 4.0 A discharge for 64 min, open-circuit for 30 min, 4.0 A charge for 64 min, open-circuit for 30 min, 4.0 A discharge to 1.0 V cut-off voltage.

effect of hysteresis phenomenon. Though some prediction errors exist, the model predictions give reasonable qualitative trends.

The cell potential with respect to time for many processes is shown in Fig. 15. The cell is fully charged first. Then the following operations are repeated on the cell: open-circuit for half an hour, discharge partially, open-circuit for half an hour, and fully charge again. The depth of discharge gradually increases for each subsequent operation. It is found that the potential of the charge process is lower than that predicted by the Nernst equation, another typical effect of the hysteresis phenomenon. However, there is good correlation between the model predictions and the experimental data for these operations.

The processes presented in Figs. 12–15 are very common operations for a nickel–metal hydride cell. However, predicting the corresponding potential behavior of the cell is very difficult due to the influence of the hysteresis phenomenon. Consequently, a model that uses a reversible nickel reaction, will encounter significant prediction errors. The model developed in this work, using the empirical approach, reflects satisfactorily the hysteresis potential behavior of the nickel–metal hydride cell.

4. Conclusions

A lumped model of a nickel–metal hydride cell was developed with attention given to many important mechanisms in the cell. One important characteristic of the nickel electrode, the hysteresis potential behavior, is described with empirical equations. The model can be used to predict the potential, pressure, and temperature behavior of a nickel–metal hydride cell for charge/open-circuit/discharge processes. The model predictions correlated well with the experimental data of a VARTA nickel–metal hydride cell. Further research work is desirable to provide a theoretical explanation of the hysteresis phenomenon of the nickel electrode.

References

[1] P.C. Milner, U.B. Thomas, in: C.W. Tobias (Ed.), Advances in Electrochemistry and Electrochemical Engineering, Vol. 5, Interscience, New York, 1967, p. 1.
[2] P. Oliva, J. Leonardi, J.F. Laurent, C. Delmas, J.J. Braconnier, M. Figlarz, F. Fievet, A. de Guibert, J. Power Sources 8 (1982) 229.
[3] G. Halpert, J. Power Sources 12 (1984) 177.
[4] R.T. Barton, P.J. Mitchell, N.A. Hampson, Surf. Coating Technol. 28 (1986) 1.
[5] G. Halpert, Nickel Hydroxide Electrodes, The Electrochemical Society Proceedings Series, Pennington, NJ, 1989, PV 90-4, p. 3.
[6] J. McBreen, in: R.E. White, J. O'M. Bockris, B.E. Conway (Eds.), Modern Aspects of Electrochemistry, Vol. 21, Plenum Press, New York, 1990, p. 29.
[7] C. Léger, C. Tessier, M. Ménétrier, C. Denage, C. Delmas, J. Electrochem. Soc. 146 (1999) 924.
[8] K.P. Ta, J. Newman, J. Electrochem. Soc. 146 (1999) 2769.
[9] K.W. Choi, N.P. Yao, in: S. Gross (Ed.), Battery Design and Optimization, The Electrochemical Society Proceedings Series, Pennington, NJ, 1979, PV 79-1, p. 62.
[10] J. Bouet, F. Richard, P. Blanchard, in: D.A. Corrigan, A.H. Zimmerman (Eds.), Nickel Hydroxide Electrodes, The Electrochemical Society Proceedings Series, Pennington, NJ, 1989, PV 90-4, p. 260.
[11] D. Fan, R.E. White, J. Electrochem. Soc. 138 (1991) 2952.
[12] J.W. Weidner, P. Timmerman, J. Electrochem. Soc. 141 (1994) 346.
[13] P. De Vidts, R.E. White, J. Electrochem. Soc. 142 (1995) 1509.
[14] S. Motupally, C.C. Streinz, J.W. Weidner, J. Electrochem. Soc. 145 (1998) 29.
[15] Q.M. Yang, M. Ciureanu, D.H. Ryan, J.O. Ström-Olsen, J. Electrochem. Soc. 141 (1994) 2108.
[16] P. De Vidts, J. Delgado, R.E. White, J. Electrochem. Soc. 142 (1995) 4006.
[17] J. Heikonen, K. Vuorilehto, T. Noponen, J. Electrochem. Soc. 143 (1996) 3972.
[18] B.S. Haran, B.N. Popov, R.E. White, J. Electrochem. Soc. 145 (1998) 4082.
[19] B. Paxton, J. Newman, J. Electrochem. Soc. 144 (1997) 3818.
[20] W.B. Gu, C.Y. Wang, S.M. Li, M.M. Geng, B.Y. Liaw, Electrochim. Acta 44 (1999) 4525.
[21] B. Wu, R.E. White, J. Power Sources 92 (2001) 177.